

Article

Performance Assessment of Irrigation Projects in Nepal by Integrating Landsat Images and Local Data

Adarsha Neupane ^{*} and Yohei SawadaDepartment of Civil Engineering, The University of Tokyo, Tokyo 113-8656, Japan;
yohei.sawada@sogo.t.u-tokyo.ac.jp^{*} Correspondence: neupane-adarsha123@g.ecc.u-tokyo.ac.jp

Abstract: With growing global concern for food and water insecurity, an efficient method to monitor irrigation projects is essential, especially in the developing world where irrigation performance is often suboptimal. In Nepal, the irrigated area has not been objectively recorded, although their assessment has substantial implications for national policy, project's annual budgets, and donor funding. Here, we present the application of Landsat images to measure irrigated areas in Nepal for the past 17 years to contribute to the assessment of the irrigation performance. Landsat 5 TM (2006–2011) and Landsat 8 OLI (2013–2022) images were used to develop a machine learning model, which classifies irrigated and non-irrigated areas in the study areas. The random forest classification achieved an overall accuracy of 82.2% and kappa statistics of 0.72. For the class of irrigation areas, the producer's accuracy and consumer's accuracy were 79% and 96%, respectively. Our regionally trained machine learning model outperforms the existing global cropland map, highlighting the need for such models for local irrigation project evaluations. We assess irrigation project performance and its drivers by combining long-term changes in satellite-derived irrigated areas with local data related to irrigation performance, such as annual budget, irrigation service fee, crop yield, precipitation, and main canal discharge.

Keywords: Landsat; random forest classification; performance assessment; irrigation; cropland map; remote sensing; satellite image



Citation: Neupane, A.; Sawada, Y. Performance Assessment of Irrigation Projects in Nepal by Integrating Landsat Images and Local Data. *Remote Sens.* **2023**, *15*, 4633. <https://doi.org/10.3390/rs15184633>

Academic Editors: No-Wook Park, Kiwon Lee and Kwangseob Kim

Received: 31 July 2023

Revised: 13 September 2023

Accepted: 19 September 2023

Published: 21 September 2023

Correction Statement: This article has been republished with a minor change. The change does not affect the scientific content of the article and further details are available within the backmatter of the website version of this article.



Copyright: © 2023 by the authors. Licensee MDPI, Basel, Switzerland. This article is an open access article distributed under the terms and conditions of the Creative Commons Attribution (CC BY) license (<https://creativecommons.org/licenses/by/4.0/>).

1. Introduction

With the rapid increase in population and growing threat of climate change, there is a global concern for food security [1–3] and water security [4]. It emphasizes the importance of proper irrigation facilities, reliable cropland maps, and agricultural intensification, particularly in developing countries whose economies are dependent on agriculture. Thus, the improvement of the performance of existing irrigation projects has become important. To improve the performance of irrigation projects, cost-efficient and objective assessments of the performance of irrigation projects are necessary.

Data of irrigated areas have various applications in diverse fields such as water resources management [5], assessment of climate change impacts on irrigation [6], and modeling water exchange in a coupled atmosphere and land surface models [7]. However, in developing countries, like Nepal, the irrigated area has been recorded non-scientifically, relying on visual inspection and local information from local people. However, the recorded irrigated area has substantial implications for donor funding, national policy, annual budgets of projects, and other relevant decision-making processes.

To improve the capability of monitoring the irrigated areas in developing countries, remote sensing serves as a promising tool because of its ability to monitor land surface conditions in a cost-effective way [8] with high accuracy [2,9]. While there are several global land use land cover (LULC) products that provide information about global cropland extent, such as Globcover (GLC; 1 km), Moderate Resolution Imaging Spectroradiometer (MODIS) land cover data (MCD12Q1; 500 m), and the European Space Agency's

land cover product (300 m) [10], numerous studies [2,11] map the global cropland extent. Pittman et al. [11] used multi-temporal MODIS data to prepare a global cropland extent map, whereas Potapov et al. [2] conducted a global analysis of cropland area changes from 2000 to 2019 using Landsat ARD (Analysis Ready Data). However, the applicability of such globally trained cropland maps for a local or regional irrigation performance assessment was unclear.

Furthermore, at local and regional scales, numerous studies have employed various machine learning algorithms on satellite-derived images to calculate irrigated areas, utilizing different types of sensors, as summarized in Table 1. However, in these studies, they either took the satellite image of a particular period or used only a single sensor to perform the time series evaluation before the classification, so that their study periods were not long enough to investigate the long-term changes in irrigation performance. Moreover, they focused only on the computation of the irrigated area without any complex quantitative analysis governing the performance of the irrigation system.

Table 1. Current trends to classify irrigated area using remote sensing.

Satellite Type	Sources	Classification Algorithm	Purpose
Landsat	[1]	Random Forest	Quantify the performance of 79 irrigation schemes across Sub-Saharan Africa for 2014–2018
	[9]	Support Vector Machine	Quantify changes in irrigated areas between 1987 and 2015 in Burkina Faso
	[12]	Maximum Likelihood	Monitor the expansion of Irrigated Areas for 1988, 2000, and 2009 in Kou Watershed
Landsat + MODIS	[13]	Single Decision Tree	Map irrigated agricultural area of Ghana for 2000–2001
	[14]	Random Forest	Monitor agricultural expansion for the years 2001, 2007, and 2014 in Burkina Faso
MODIS	[15]	Single Decision Tree	Develop high-resolution irrigated area map of India for 2000 to 2015
	[16]	Single Decision Tree	Map annual irrigated areas in Afghanistan from 2000 to 2013
	[17]	Unsupervised	Map irrigated area of Krishna River Basin, India for 2000–2001
Landsat + Sentinel-2	[18]	Random Forest Support Vector Machine Boosted Decision Tree Single Decision Tree Artificial Neural Network k-Nearest Neighbor	Comparison of six supervised classification approaches in the detection of irrigated areas in Southern Italy and found Random Forest as one of the best performers

It is beneficial to evaluate the performance of irrigation projects and its drivers by integrating satellite-based irrigation maps and other local data. The performance of several irrigation projects has been assessed utilizing both remotely sensed irrigation performance indicators, such as relative evapotranspiration, delivery performance ratio, drainage ratio, depleted fraction, crop water productivity, and so on by [19–21], and socio-economic indicators, such as grain yield, price ratio, and water productivity by [22]. Kumar [23] and Nikam et al. [24] combined the remote-sensing-based estimates with the water release data from the project and other field observations data. Similarly, Higginbottom et al. [1] examined the relationship between irrigation scheme performance and explanatory variables, the underlying drivers, with a tendency to over-promise and under-deliver in scheme planning for irrigation schemes of Sub-Saharan Africa. However, a thorough evaluation of an irrigation project’s performance and its drivers have not been carried out by comparing

the irrigation performance indicators based on relevant local data with the satellite-derived irrigation area.

In the context of Nepal, national-scale agricultural land cover maps were developed using MODIS 250 m NDVI time series data for the year 2016 [25], temporal rice-growing area and land-use change maps were provided using MODIS 500 m time series data [26], and 30 m resolution maps were generated through land suitability assessments and a land allocation model [27]. However, there is a gap in the availability of local-level cropland maps utilizing high-resolution satellite imagery for evaluating long-term changes in cropland areas. Additionally, while several studies assessed the performance of irrigation projects in Nepal [28–30], these assessments primarily focused on the physical structure and institutional performance of Water User’s Associations, the effects of engineering infrastructure and governance structure, or the examination of the design aspects of irrigation systems. A comprehensive assessment of irrigation projects using irrigation performance indicators and local data has not yet been conducted.

Within this context, the objectives of this study were to

- Develop a locally trained cropland classification map and quantify changes in cropland areas from 2006 to 2022 using Landsat 5 TM and Landsat 8 OLI for irrigation projects in Nepal;
- Assess the performance of irrigation projects by utilizing remote-sensing-derived irrigated area data in conjunction with local data;
- Analyze the effectiveness of global datasets at the local or regional levels by comparing the global cropland map with our locally trained map.

In Section 2, we show the location map of the irrigation projects selected for this study. In Section 3, we first describe the relevant data used and the general image preprocessing steps, and then, we discuss the methodology used to classify irrigated areas from non-irrigated ones. Subsequently, in Section 4, we present the results, including locally trained cropland classification maps obtained from the study, accuracy assessments, comparisons with the global cropland map, and the variables used to assess the performance of the irrigation project. Next, in Section 5, the Discussion section, we compare the findings of this study with previous studies and discuss the limitations and implications of the applied techniques. Finally, in the last section of the paper, we draw conclusions from the study.

2. Study Area

Sunsari–Morang Irrigation Project (SMIP) is the largest irrigation project in Nepal, whose command area is 68,000 ha. We focused on SMIP to collect training and validation points to develop our cropland classification method. To check the robustness of the methodology, our developed methods were also applied to the Bagmati Irrigation System (BIS), Nepal’s second-largest irrigation project with a command area of 45,600 ha. Figure 1 shows the location of these two irrigation projects. During monsoon-driven agricultural season, typically known as Kharif season in South Asia, the irrigated areas of SMIP and BIS, recorded by the Department of Water Resources and Irrigation, Nepal, were 66,000 ha and 39,700 ha, respectively, for every year since 2010 [31] (p. 73), [32] (p. 55), [33] (p. 62), [34] (p. 64), [35] (p. 67), [36] (p. 65), [37] (p. 71), [38] (p. 81), [39] (p. 79), [40] (p. 83), [41] (p. 87). These irrigated areas are, in fact, recorded non-scientifically by the authorized governmental body.

In both regions, farmers grow a variety of crops throughout the year. Major field crops in these areas are paddy, wheat, maize, sugarcane, and several other vegetable crops. In Nepal, a subsistence-based economy, most farmers use the staple crop, paddy, as their primary production, especially in the Kharif season. Due to the reliability of irrigations service in the Kharif season, supported by the rainfall due to the ongoing monsoon, the farmers of the study areas plant paddy as their principal crop during this season. During the Kharif season, the usual planting dates for paddy vary from June to July, and harvesting dates are from late September to early November.

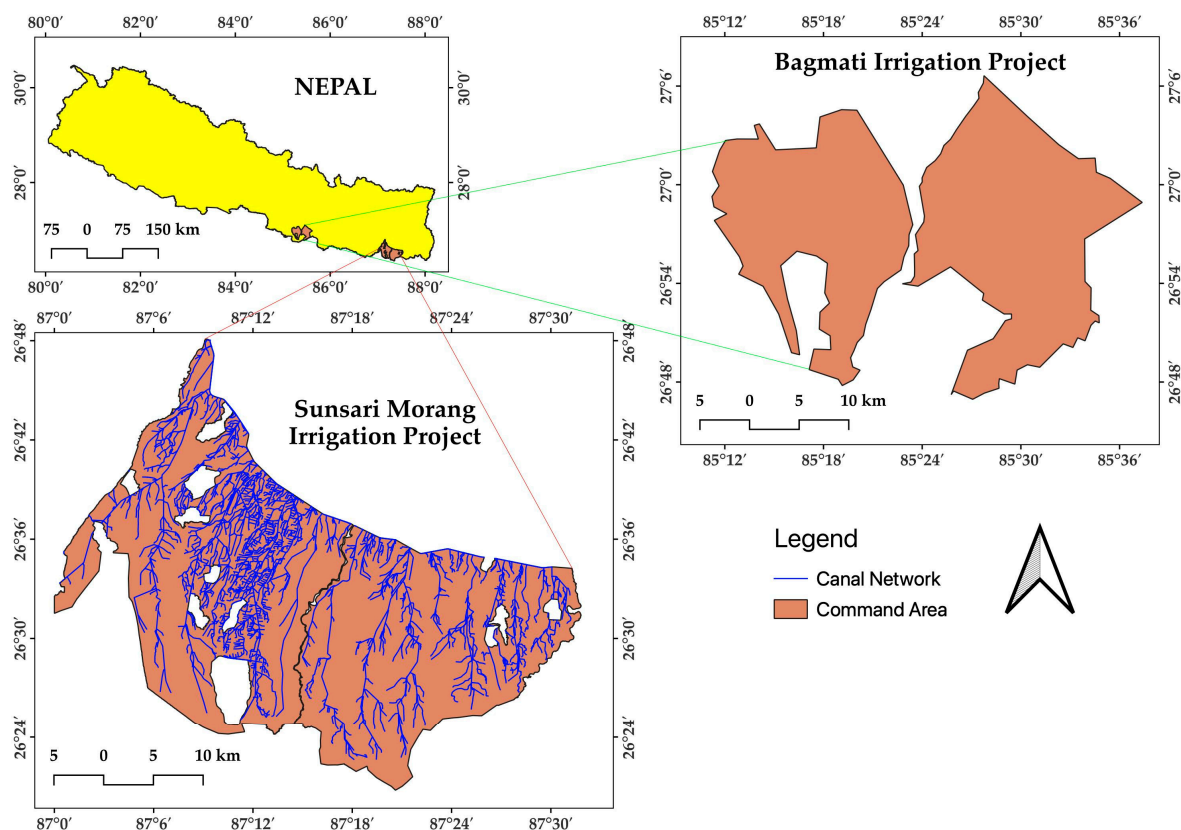


Figure 1. Location map of the study area.

3. Materials and Methods

3.1. Methodological Framework

In our proposed method, the cropland classification maps from 2006 to 2022 in the study areas were provided using the Random Forest classifier in the Google Earth Engine platform. We focused on classifying irrigated areas for paddy so that Landsat images for July to October, the growing season of paddy, were collected throughout the study period. Typically, there is an active monsoon during the majority of chosen time; thus, almost all the satellite images retrieved in this study had cloud cover. Cloud masking was performed in every image to make cloud-free composites. Depending upon the quality of the cloud-free image collections, the cloud-free composites were grouped as 2-year period in the case of Landsat 8 OLI and 3-year period in the case of Landsat 5 TM. The image composites were enhanced by adding NDVI and EVI bands, as those spectral indices were highly sensitive to vegetation. Spectral matching of Landsat 5 TM images with the reference image, obtained by taking the median of Landsat 8 OLI image collections from 2013–2014 to 2021–2022 periods, was performed using NDVI and EVI bands. The median image of those enhanced image composites was used for classification using the Random Forests classifier. Training points were taken from high-resolution Google Earth images and Landsat 8 2021–2022 images for three different classes: Agriculture, Forest/Pastures, and Non-Agriculture. Those training points were used to train the classifier. After that, the classified images were smoothed to remove the noises and enhance the image's visual quality. Then, the irrigated area was separated from the non-irrigated area, and the sum of pixels classified as Agriculture class in the smoothed image was designated as the total irrigated area.

The irrigation project's performance assessment was performed using the cropland classification maps and variables collected from various sources. The delivered irrigated area from the classified satellite imageries was compared with the irrigated area recorded by the authorized governmental body, the Department of Water Resources and Irrigation

(DWRI). The discrepancy in those two irrigated areas was analyzed. The overall assessment of the irrigation projects was performed by comparing the satellite-derived irrigated area with various variables such as yield, irrigation service fee (ISF), project annual budget, main canal discharge, and amount of precipitation contributing to the command area. Those variables included (1) socio-economic performance indicators: yield and ISF and (2) factors that influenced the performance of an irrigation project: project annual budget, main canal discharge, and amount of precipitation. Figure 2 shows the general overview of the proposed method.

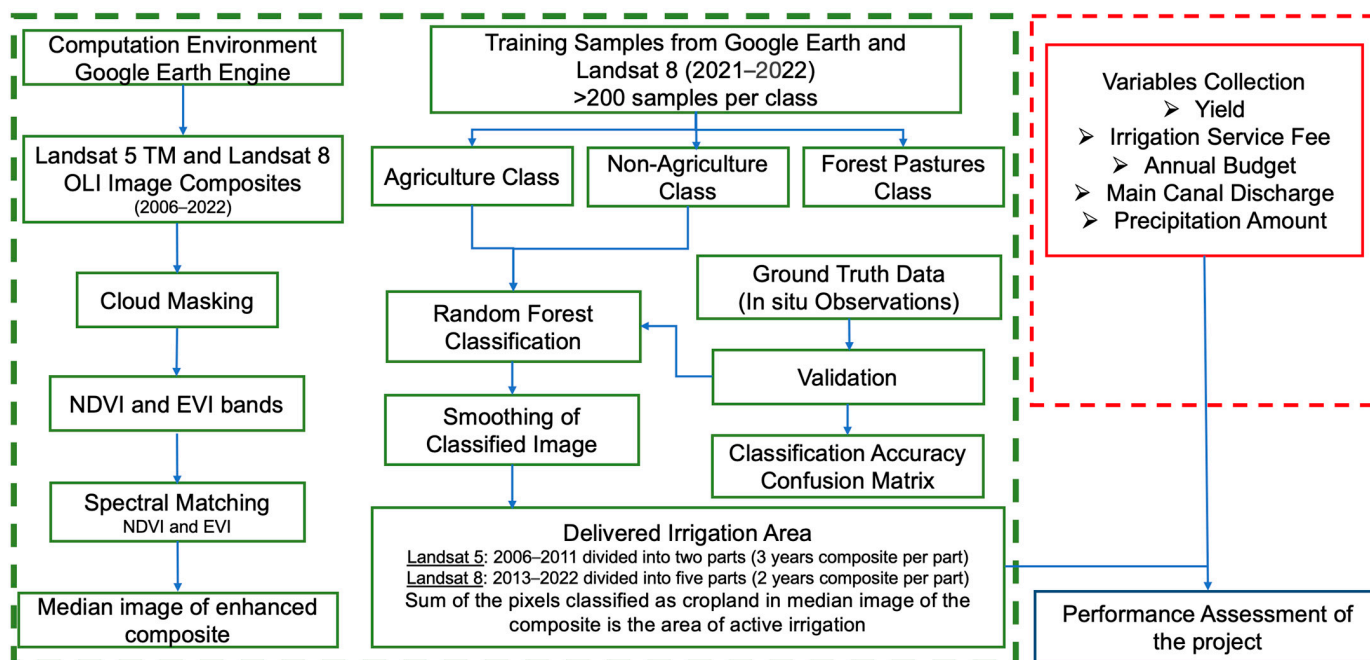


Figure 2. General overview of the study.

3.2. Remote Sensing

3.2.1. Data Used

We used Landsat 5 TM and Landsat 8 OLI surface reflectance Level 2, Collection 2, and Tier 1 image collections from July to October for the time series evaluation of the irrigation projects. Those images were downloaded from Earth Engine Data Catalog [42,43] from United States Geological Survey (USGS). Blue, Green, Red, and Near-Infrared (NIR) bands were used for the image classification, and a QA_PIXEL band was used for masking the clouds. Landsat 5 TM image collections were used from 2006 to 2011, and Landsat 8 OLI from 2013 to 2022. Due to the unavailability of images in 2012, no analysis was performed for that particular year. Through visual interpretation, the training samples were manually selected using high-resolution Google Earth imagery along with the Landsat 8 metrics for the 2021–2022 period [1,2]. The GPS coordinates were collected during the field visit to the project's command area, which was later used for validation.

3.2.2. Google Earth Engine

We used the Google Earth Engine (GEE) cloud environment for the entire assessment, which includes satellite image visualization, classification, and command area computation of this study. GEE is a cloud-based platform that provides the capability to retrieve massive satellite images and perform advanced image processing using machine learning algorithms, enabling scientific analysis and visualization of geospatial datasets [44,45].

3.2.3. Image Preprocessing

We used atmospherically corrected surface reflectance derived from the data produced by Landsat 5 TM and Landsat 8 OLI. Such Level 2 surface reflectance products already include several preprocessing steps, such as atmospheric correction, which enhances the usability of the data for various applications. However, image mosaicking, cloud masking, and implementation of the scaling factor were necessary before the images were used for further analysis and classification.

Image Mosaicking

To create a cohesive and continuous composite image for the study area, image mosaicking, which involves combining multiple satellite images [46], was conducted. The study area, Sunsari–Morang Irrigation Project (SMIP), falls on two Landsat tiles, having a path/row combination of 140/41 and 140/42. That is why the region of interest (ROI) was defined to cover the entire study area, including the mosaicked images. The image mosaicking was implemented in GEE. However, Bagmati Irrigation System (BIS) only falls on one Landsat tile—141/41. In this case, we defined the region of interest without performing the image mosaicking.

Cloud Masking

The satellite images used in this study were masked for cloud cover before classification and further analysis. Cloud masking aims to separate cloud pixels from the rest of the image, allowing for a more accurate and reliable analysis of the underlying features. Since the study area had monsoon seasons throughout the study period from July to October, most of the images had cloud cover, making it challenging to obtain cloud-free images that could be used for cropland classification. Thus, the cloud masking algorithm was employed for masking the clouds. A binary mask was created for Bit 0, Bit 1, Bit 2, Bit 3, and Bit 4 of the QA_PIXEL band for both Landsat 5 TM and Landsat 8 OLI. Similarly, a binary mask was also created for the QA_RADSAT band for both satellites.

Scaling Factor

The optical and thermal bands were converted from digital number (DN) to reflectance and brightness temperature, respectively, using the scaling factor in this study prior to further analysis and classification of the image. The data provided for ‘Scale’ and ‘Offset’ for various optical and thermal bands on the Earth Engine Data Catalog for both the satellites, [42] for Landsat 5 TM and [43] for Landsat 8 OLI, were used for this operation.

3.2.4. Image Composites

We took two years of image composites for Landsat 8 OLI and three years for Landsat 5 TM. From several sensitivity analyses, we found two years of cloud-free image composites yielded a complete image throughout the composite periods, a total of five, from 2013 to 2022 for Landsat 8 OLI. However, the three-year cloud-free image composite only yielded a reasonable result for Landsat 5 TM for two composite periods from 2006 to 2011. No retrievable image was available for 2012 in Landsat 5 TM, so this particular year was neglected in our study.

3.2.5. Spectral Indices

We chose spectral indices, NDVI and EVI, which are highly sensitive to vegetation’s presence and vigor. NDVI has been widely used as an indicator for irrigated areas [18] since it detects changes in vegetation reflectance, especially for the forest, agriculture, and crop types [15]. Similarly, EVI for cropland mapping [8] can provide valuable insights into vegetation conditions, stress levels, and crop health. Thus, NDVI and EVI bands were added to the original bands of the collection of images grouped as cloud-free image composites, and enhanced collection composites were obtained. Then, the median images for each enhanced collection composite were computed and used for classification.

3.2.6. Spectral Matching

Spectral matching [26,47] was performed on enhanced image composites of Landsat 5 TM before classification. We obtained unsatisfactory results when we directly applied the same classifier trained with high-resolution Google Earth image and Landsat 8 OLI image to Landsat 5 TM images due to the differences in spectral characteristics between the two satellite sensors.

To address this issue, a two-step approach was taken. Firstly, a reference image was obtained by computing the median of all the enhanced image composites for Landsat 8 OLI. Secondly, the NDVI and EVI bands of the enhanced images of Landsat 5 TM were then subtracted and multiplied from the corresponding NDVI and EVI bands of the reference image. The NDVI difference and NDVI ratio were applied to the NIR band of Landsat 5 TM enhanced image, producing a matched NDVI band. The same technique was applied to compute the matched EVI band. Adding these matched NDVI and EVI bands to the Landsat 5 TM enhanced image composites, a set of matched image composites suitable for classification was obtained.

The NIR band was explicitly chosen for spectral matching due to its significance in vegetation analysis, as it captures the reflectance of healthy vegetation, which is typically higher in the NIR region. Applying spectral matching to the NIR band aims to ensure consistent and comparable spectral information related to vegetation, including crops, across different images. This process enhances the accuracy and comparability of cropland classification by reducing spectral variations and ensuring consistent representation of vegetation-related features across different images or datasets.

3.2.7. Feature Extraction

The extraction of features for the training dataset was performed, covering the spatial extent of the entire study for the 2021–22 period. The training points were collected for three classes: Agriculture, Non-Agriculture, and Forest/Pastures. The number of training samples used per class was

- Agriculture class—424;
- Non-Agriculture class—898;
- Forest/Pastures class—222.

3.2.8. Cropland Classification

We performed the cropland classification of the median image using the Random Forest (RF) classifier [1,8,10], a supervised classification technique. The RF classifier's accuracy and output were insensitive to variations in the number of trees and the maximum depth of each tree. This feature demonstrates the classifier's robustness against overfitting in various settings. We performed the experiments with the various combinations, including 50/50, 75/75, 100/75, 100/100, 200/100, 200/200, 500/100, and 1000/100 for the number of trees and maximum depth. The overall accuracy (OA) ranged from 0.809 to 0.8219, kappa metrics from 0.697 to 0.721, and Out-of-Bag Error Estimate from 0.126 to 0.136 for these combinations. Notably, when the number of trees was tuned to 200 and the maximum depth of each tree was set to 75, a slightly better result was obtained with an overall accuracy (OA) of 82.19%, kappa coefficient of 0.721, and Out-of-Bag Error Estimate of the classifier at 0.1258, compared to different combinations of these parameters. We show the results obtained by this hyperparameter set in this paper.

3.2.9. Smoothing of Classified Image

We performed spatial smoothing (neighborhood mode), which includes erosion and dilation. The circular kernel of radius 1 was slid through the image. During erosion, a pixel in the original image (1 or 0) was considered 1 only if all the pixels under the kernel were 1. Otherwise, it was eroded (made to 0). Through this process, all the pixels near the boundary were discarded, decreasing the foreground object's thickness or size. It helped remove small noises.

Dilation is conceptually opposite to erosion. A pixel element was considered 1 if at least one pixel under the kernel was 1. It increased the size of the foreground object. Totally, two iterations were performed for both the erosion and dilation processes during the smoothing operation.

3.2.10. Delivered Irrigation Area

The irrigated area map was created by separating irrigated and non-irrigated areas from the smoothed image. The Agriculture class of the smoothed image was separated from the other two classes: Non-Agriculture class and Forest/Pastures class. The area covered by the Agriculture class was designated as irrigated area, whereas the other two classes were designated as non-irrigated areas. We assumed that the Agriculture class is associated with irrigation water supply in our study areas. Subsequently, a binary map of the irrigated area was generated for the study period.

3.2.11. Validation

The ground truth samples collected during the field visit from March 6 to March 15, 2023, were used to validate the classification result. GPS coordinates representing all three classes (Agriculture, Non-Agriculture, and Forest/Pastures) were collected during the visit. While collecting the coordinates, we made sure that the ground truth samples included the data from head- to tail-end of the command area and are representative of both Sunsari and Morang districts to minimize any biases in the data. The number of the validation samples collected per class was

- Agriculture class—290;
- Non-Agriculture class—139;
- Forest/Pastures class—127.

3.2.12. Accuracy Assessment

In this study, overall accuracy (OA), producer's accuracy (PA), consumer's accuracy (CA), and kappa coefficient (\hat{k}) were used to assess the accuracy of Random Forest classifier [10,48–53]. The classifier's overall accuracy was assessed by dividing the total count of pixels that were correctly classified by the total count of reference pixels, as shown in Formula (1) [10]. Producer's accuracy, shown in Formula (2) [10], for each category was calculated by dividing the number of correctly classified pixels in each category (found along the major diagonal; see Table 2) by the total count of test set pixels used for that specific category (the column total; see Table 2). On the other hand, consumer's accuracy was determined by dividing the number of correctly classified pixels in each category belonging to that category by the total count of pixels in that category's row and is provided in Formula (3) [10].

$$OA(\%) = \frac{\Sigma \text{ Number of pixels correctly classified}}{\text{Total count of reference pixels}} \quad (1)$$

$$PA(\%) = \frac{\text{Number of pixels correctly classified in a class}}{\text{Number of training pixels in that class}} \quad (2)$$

$$CA(\%) = \frac{\text{Number of pixels correctly classified in a class}}{\text{Total number of pixels classified in that class}} \quad (3)$$

The kappa statistic was computed using the following formula [50]:

$$\hat{k} = \frac{N \sum_{i=1}^r x_{ii} - \sum_{i=1}^r (x_{i+} \cdot x_{+i})}{N^2 - \sum_{i=1}^r (x_{i+} \cdot x_{+i})} \quad (4)$$

where

r = number of rows in the error matrix;

x_{ii} = number of observations in row i and column i ;

x_{i+} = total number of observations in row i ;
 x_{+i} = total number of observations in column i ;
 N = total number of observations included in matrix.

Table 2. Confusion Matrix.

Class	Agriculture	Forest/Pastures	Non-Agriculture	Row Total	Consumer's Accuracy
Agriculture	228	9	1	238	0.96
Forest/Pastures	53	125	22	200	0.63
Non-Agriculture	9	5	104	118	0.88
Column Total	290	139	127	556	
Producer's Accuracy	0.79	0.90	0.82		

Overall accuracy = 82.20%; kappa coefficient = 0.72.

3.3. Performance Assessment of Irrigation Projects

Our performance assessment of irrigation projects includes the evaluation of irrigation performance, its drivers, and the value added by the irrigation systems. ISF was used as the proxy of the irrigation performance, whereas paddy yield represents both the performance indicators and the value for farmers added by the irrigation system. Both the data of ISF collected from the project's beneficiary farmers [31] (p. 82), [32] (p. 62), [33] (p. 69), [34] (p. 69), [35] (p. 72), [36] (p. 70), [37] (p. 76), [38] (p. 86), [39] (p. 84), [40] (p. 88), [41] (p. 92), and paddy yield (MT/ha) for the Kharif season [31] (p. 86), [32] (p. 67), [33] (p. 74), [34] (p. 74), [35] (p. 76), [36] (p. 74), [37] (p. 80), [38] (p. 90), [39] (p. 88), [40] (p. 92), [41] (p. 96) were obtained from the DWRI, Nepal. National average yield of paddy [54] (p. 5), [55] (p. 11), and [56] was also obtained from the Ministry of Agricultural Development (MoALD) of Nepal. The variables that impact the project's performance, which we call drivers, such as amount of precipitation, project's annual budget [31] (p. 73), [32] (p. 55), [33] (p. 62), [34] (p. 64), [35] (p. 67), [36] (p. 65), [37] (p. 71), [38] (p. 81), [39] (p. 79), [40] (p. 83), [41] (p. 87), and discharge in the main canal, were collected. Monthly (July to October) precipitation data from five rainfall stations that lied within or contributed to the command area runoff were collected from the Department of Hydrology and Meteorology (DHM), Nepal. Discharge of the main canal was obtained from the project office. The monetary variables, i.e., ISF and the project's annual budget, were converted using Consumer Price Index (CPI), taking the year 2014.15 as the base period according to the guidelines provided by Nepal Rastra Bank (NRB), the central bank of Nepal [57] (p. 419), [58] (p. 447).

4. Results

4.1. Accuracy Assessment of the Classifier

Table 2 shows the confusion matrix obtained from the classified map 2021–2022 to evaluate the performance of our classifier. The overall accuracy and kappa coefficient were 82.2% and 0.72, respectively. The producer's and consumer's accuracies for the Agriculture class, the class used to separate the irrigated area in this study, were 79% and 96%, respectively. The Non-Agriculture class had consistently better accuracies, with both producer's and consumer's accuracies above 80%; however, there was greater variability in the Forest/Pastures class. This class had an excellent producer's accuracy of 90%, whereas the consumer's accuracy was insufficient (63%). In fact, the 53 samples of the Agriculture class were misclassified, thus resulting in a lower producer's accuracy for the Agriculture class (79%) and lower consumer's accuracy for the Forest/Pastures class (63%). From the spectral signature shown in Figure 3, the spectral characteristics of the Agriculture class and Forest/Pastures class were similar, although the Agriculture class had a slightly higher reflectance value in the NIR region. This is why the samples of the Agriculture class were usually misclassified as the Forest/Pastures class.

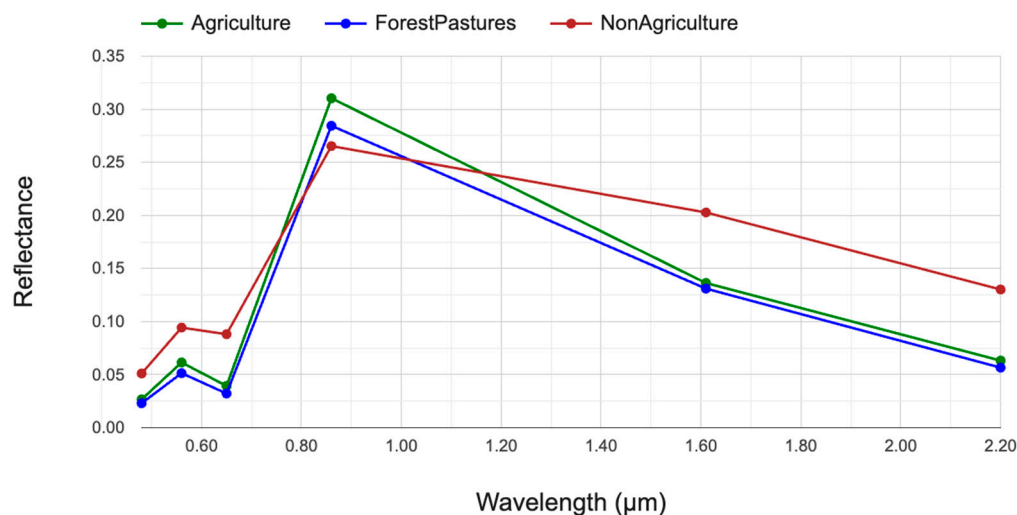


Figure 3. Spectral Signature by class.

4.2. Cropland Classification

The cropland classification maps were obtained for the study areas by separating the irrigated areas from non-irrigated ones. Figure 4 shows the cropland classification maps of SMIP from 2006 to 2022, where the classified image obtained from Landsat 5 TM was represented in a three-year period, i.e., 2006–2008 and 2009–2011, and for the one obtained from Landsat 8 OLI, in a two-year period—2013–2014, 2015–2016, 2017–2018, 2019–2020, and 2021–2022. There are two important implications in Figure 4. First, the tail-end portion, the southern part of the command area, was not fully irrigated although some improvements can be found in the later years (2017–2018 and 2021–2022 periods). The tail-end portions of the command area lack irrigation facilities necessary for surface irrigation. However, the gradual increment in 2017–2018 and 2021–2022 shown in Figure 4 implies that the irrigation system was adequately managed and there was proper water management. Second, the irrigated area in the 2019–2020 period significantly declined especially in the eastern part of the command area of the project. This is because the major flood occurred in 2017 [59], which damaged the aqueduct of the main canal, which deprives the irrigation facility in that part of the command area.

Figure 5 shows the cropland classification maps of BIS from 2013 to 2022. Due to the unavailability of good-quality images obtained from Landsat 5 TM for the command area during the study period 2006 to 2012, the satellite images obtained from Landsat 8 OLI were only used. We found that the area under agriculture significantly increased in 2017–2018, 2019–2020, and 2021–2022 compared to the initial years.

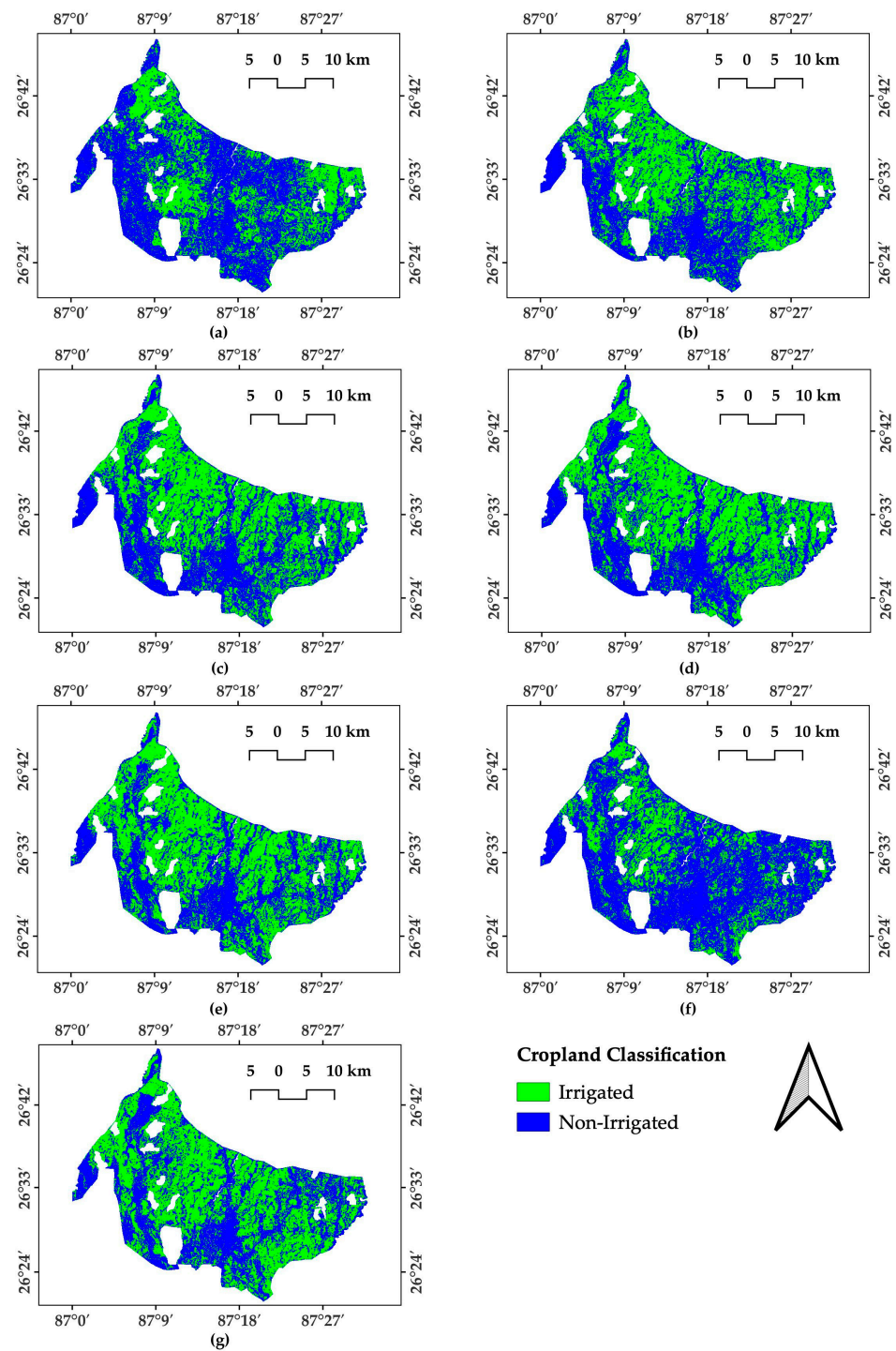


Figure 4. Cropland Classification Maps of BIS showing temporal changes in irrigated area throughout the study periods: (a) 2006–2008; (b) 2009–2011; (c) 2013–2014; (d) 2015–2016; (e) 2017–2018; (f) 2019–2020; and (g) 2021–2022.

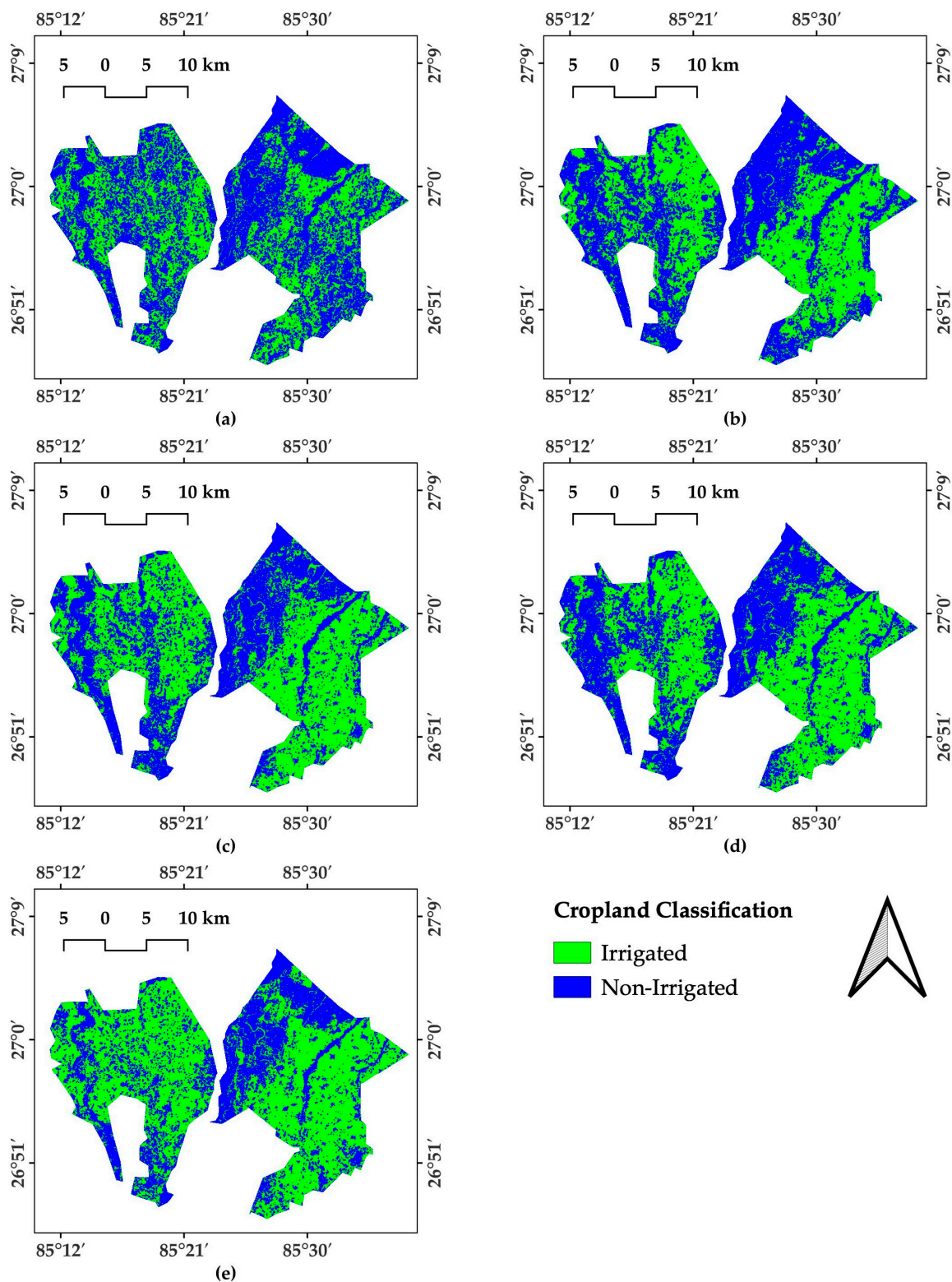


Figure 5. Cropland Classification Maps of BIS showing temporal changes in irrigated area throughout the study periods: (a) 2013–2014; (b) 2015–2016; (c) 2017–2018; (d) 2019–2020; and (e) 2021–2022.

4.3. Recorded vs. Satellite-Derived Irrigated Areas

Figure 6 compares the satellite-derived irrigated area and the irrigated area recorded by the DWRI for both SMIP and BIS throughout the study period. The irrigated area of the irrigation projects obtained from our cropland classification maps substantially changes

over time. However, DWRI reported the constant values of irrigated area, which were 66,000 ha for SMIP and 39,700 ha for BIS during the Kharif season. In the case of SMIP, the satellite-derived irrigated area was less than the area recorded by the DWRI by at least 8000 ha every year. As we discussed, the total irrigated area increased from 2006 to 2018 and suddenly declined in the 2019–2020 period due to the effect of flooding. The dynamics of the irrigated area were not recorded by the DWRI. For BIS, the irrigated area consistently improved over the years, surpassing the DWRI's recorded values for the 2017–2018 and 2021–2022 periods. It indicates a significant achievement by BIS in expanding the irrigated area, which has been overlooked by DWRI.

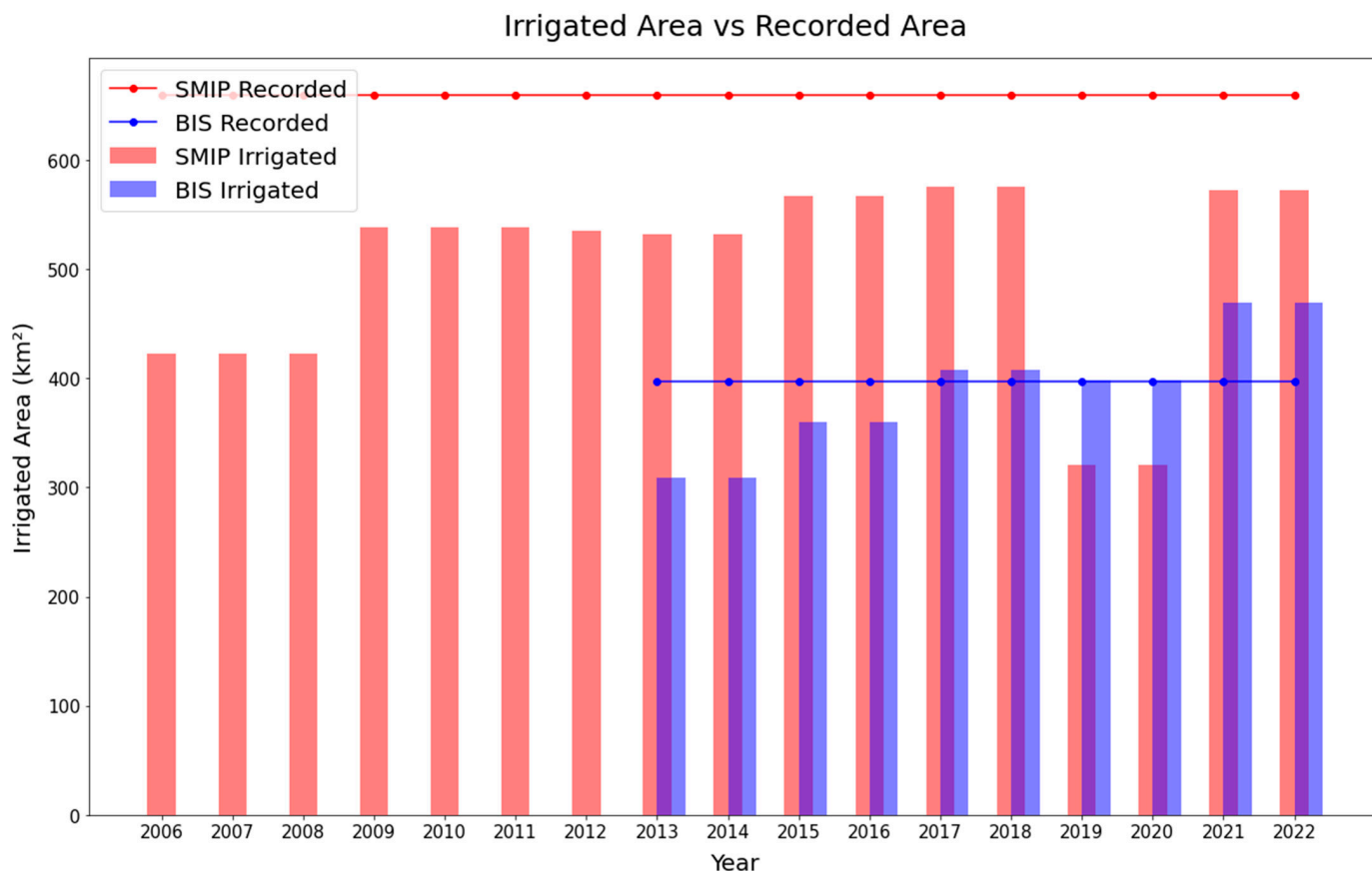


Figure 6. Comparison of DWRI recorded and satellite-derived irrigated areas.

4.4. Comparison of Classification Result with Globally Trained Cropland Classification

Our cropland classification map trained by the local dataset is substantially different from the globally trained cropland classification map provided by [2]. When the Global Cropland Classification Map (GCCM) provided by [2] was compared with our estimated cropped area, as shown in Figure 7, GCCM classified most of the command area as stable cropland, which was inconsistent to our findings. Regarding the tail-end portions of the command area, the globally trained cropland classification map overestimated the cropland area throughout the study period, as shown in Figure 7a–f. Most importantly, the global cropland map only showed a minor change in the cropland area throughout the study period, and it did not replicate the cropland area loss caused by a major flood event in 2019–2020, as shown in Figure 7f. These results indicate that an existing global cropland map cannot accurately reproduce the small-scale distribution of irrigated land.

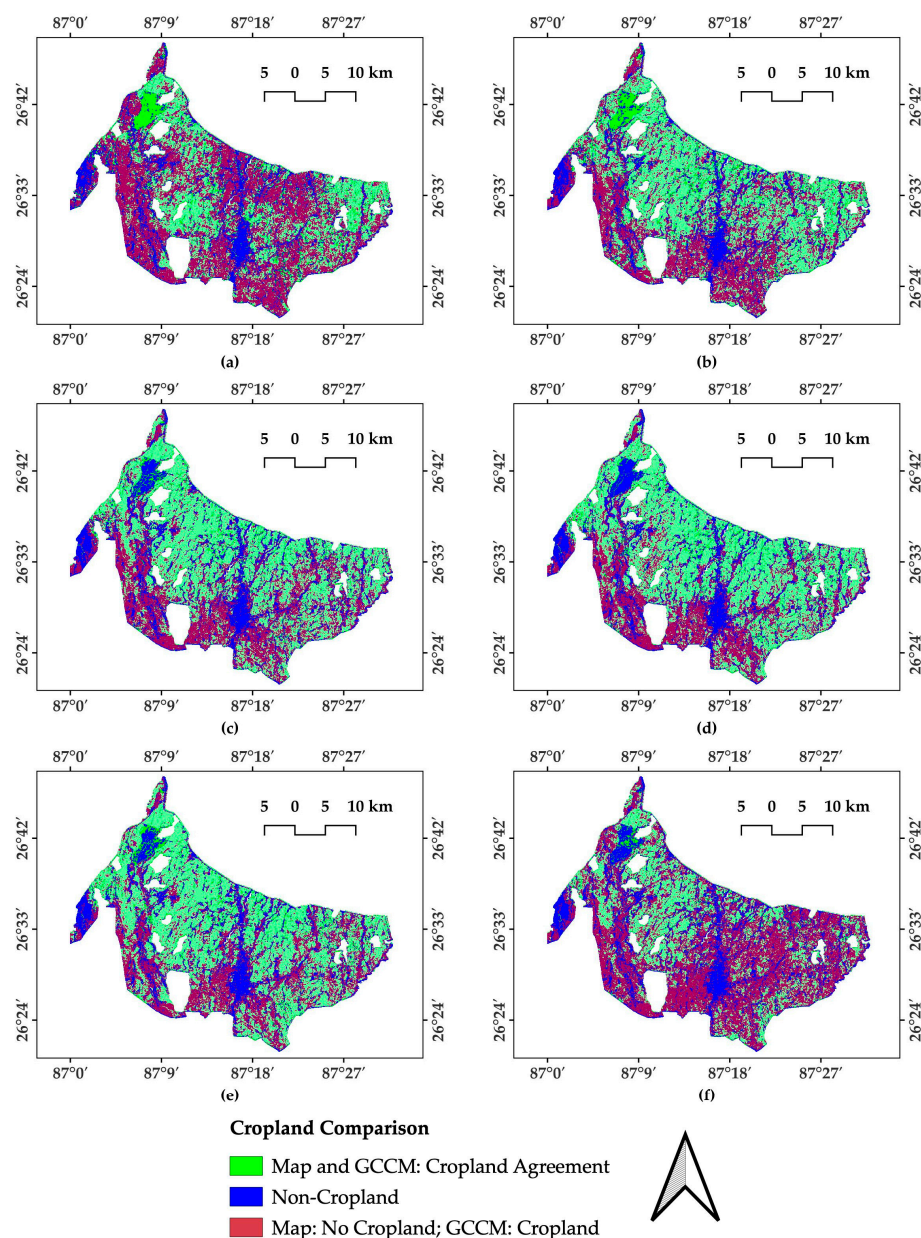


Figure 7. Comparison of Global Cropland Classification Maps (GCCMs) clipped for the study area (SMIP) with the Cropland Classification Maps obtained from this study throughout the study periods: (a) 2006–2008; (b) 2009–2011; (c) 2013–2014; (d) 2015–2016; (e) 2017–2018; and (f) 2019–2020.

4.5. Performance Assessment of the Project

4.5.1. Performance Indicators

Socio-economic indicators were used to assess the performance of the projects. For that purpose, paddy yield and ISF of the command area were compared with the irrigation area discussed above.

Yield

Figure 8 shows the time series of paddy yield, measured in metric ton per hectare (MT/ha) with the change in irrigated area. As far as SMIP is concerned, the annual yield of paddy was meager in the year 2009–2010; however, with the increase in irrigated areas, there was almost a linear increase till 2019–2020. The SMIP irrigation project successfully increased not only irrigated areas, but also the production performance per area. For BIS, the yield remained relatively constant until 2019–2020, although in the last two years,

2020–2021 and 2021–2022, there was an increase in yield, accompanied by an increase in the irrigated area. As the cropped area expanded, there was a tendency for higher yields.

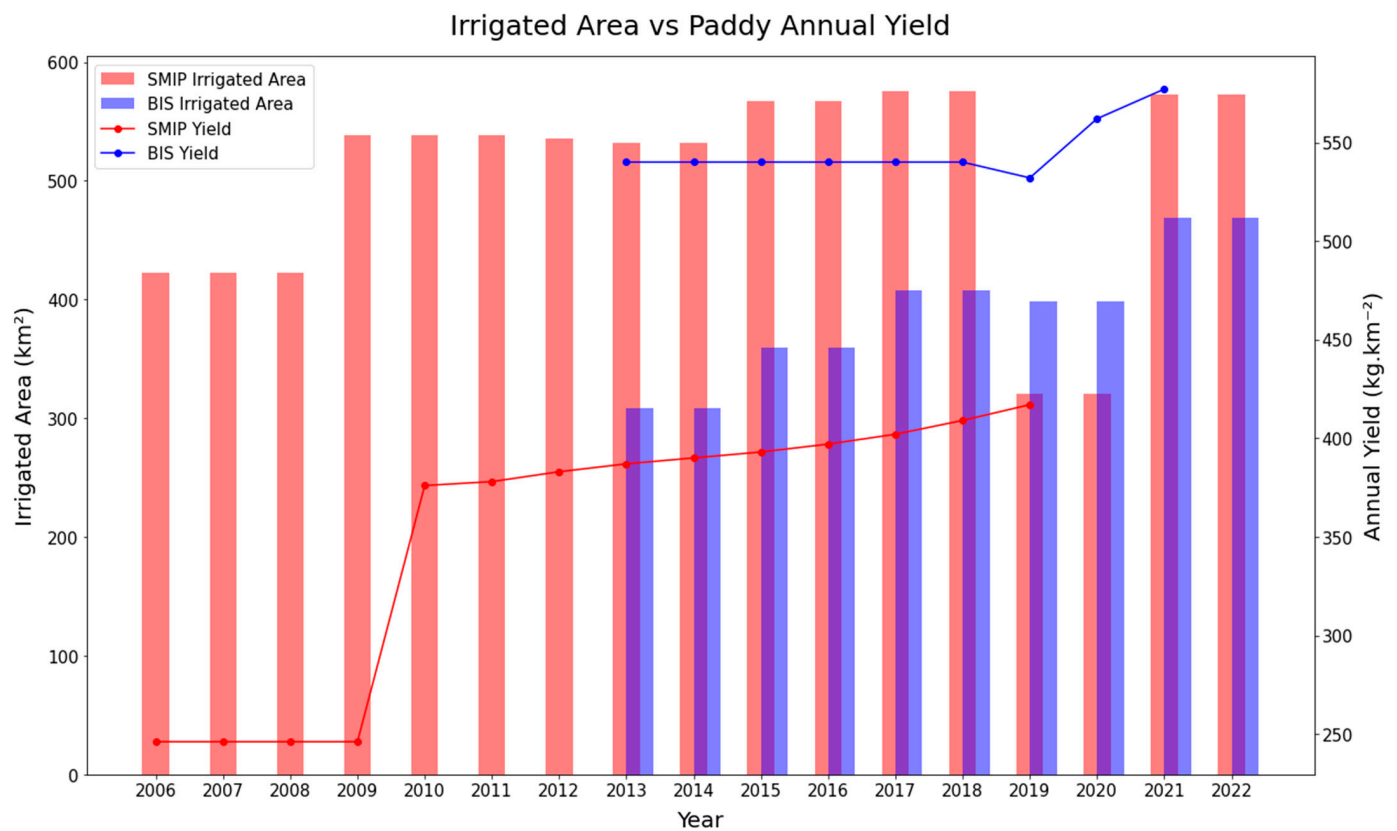


Figure 8. Impact of Irrigated Area on Paddy Yield.

The provision of irrigation facilities substantially improved the paddy yield compared to the ones that did not acquire those facilities, thus justifying the value added by those irrigation projects. Figure 9 compares the projects' annual paddy yields (MT/ha) with the national average. There was an increase in paddy yield over time, with an almost linear trend observed across all three sectors: SMIP, BIS, and national average. Both irrigation projects consistently showed higher yields than the nationwide-averaged yield, with only one exception for SMIP in 2009–2010 when the yield was less by 0.255 MT/ha compared to the national average. In the case of BIS, this difference with the national average reached as high as 2.246 MT/ha during 2015–2016.

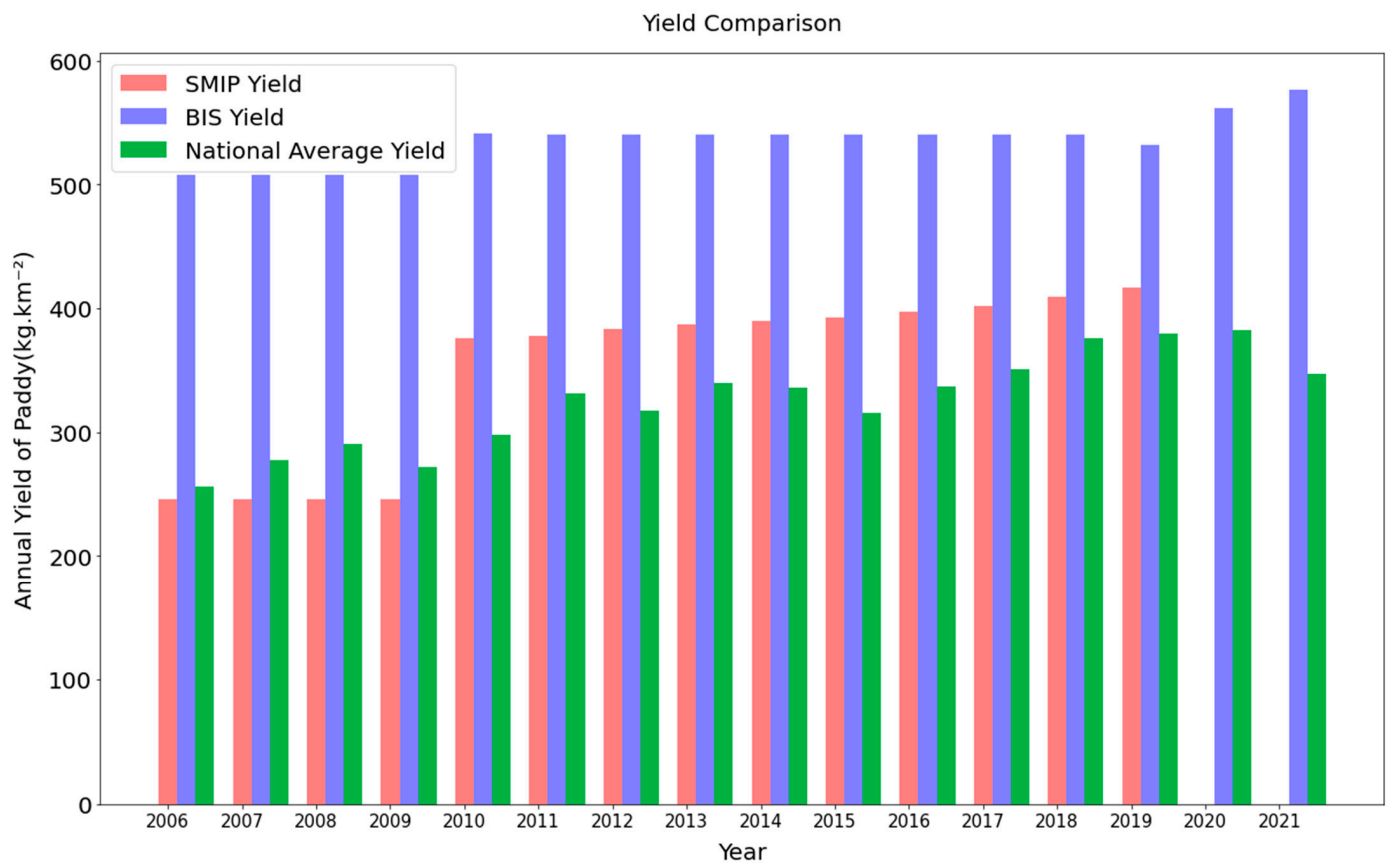


Figure 9. Comparison of project annual yield with national average yield.

Irrigation Service Fee Collection

Fluctuations in the collection of ISF can be seen in both the irrigation projects, SMIP and BIS, as shown in Figure 10. In the case of SMIP, there was a significant fluctuation in ISF throughout the study period, with the least ISFs collected in 2011–2012. After 2012, the ISF collection improved almost linearly till reaching the peak in 2016–2017, accompanied by the project office's delivery of constantly increased irrigated areas. This was followed by a sharp drop till 2019–2020 due to decreased irrigated areas. With an increase in the irrigated areas in 2021–2022, there was a significant improvement in ISF collection. In the case of BIS, although there was an almost linear increase in the irrigated area throughout the study period, the ISF collection displayed a different trend. There was an increase in the second year of collection compared to the first year (2015–2016), which remained relatively constant the following year. Then, there was a steep drop in 2018–2019, followed by a linearly increasing trend. One of the reasons behind this could be the reduction in the annual budget allocated to BIS for 2019–2020 (refer to Figure 11). Generally, in Nepal, the ISF of a particular year is collected at the end of that fiscal year. In contrast, the annual budget for the upcoming year is allocated at the end of the previous fiscal year. Therefore, the annual budget of BIS for 2019–2020 was allocated at the end of 2018–2019, and a sharp decline in this value may have impacted the farmer's reluctance to give the ISF, thus reducing ISF collection for 2018–2019.

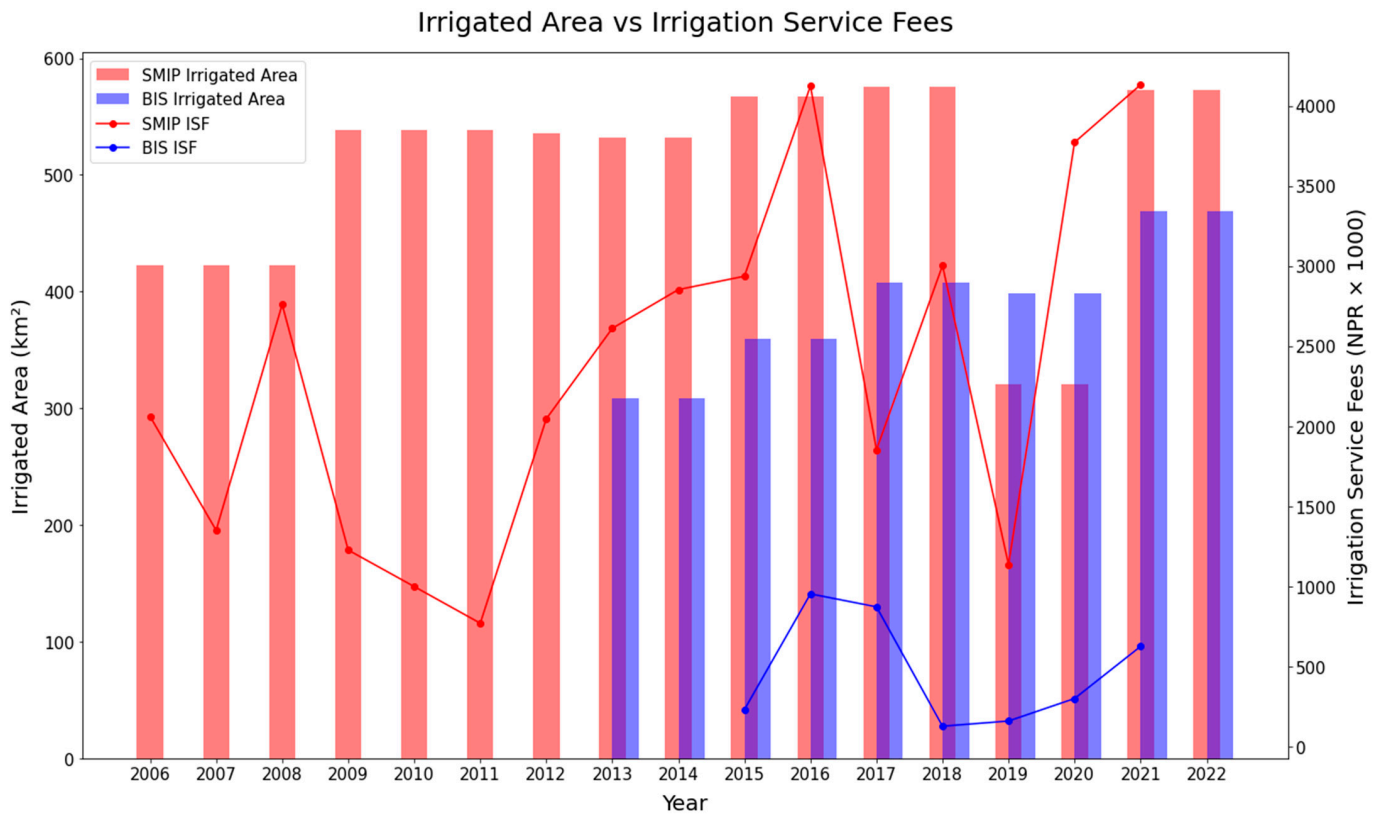


Figure 10. Variation in ISF collection with Irrigated Area.

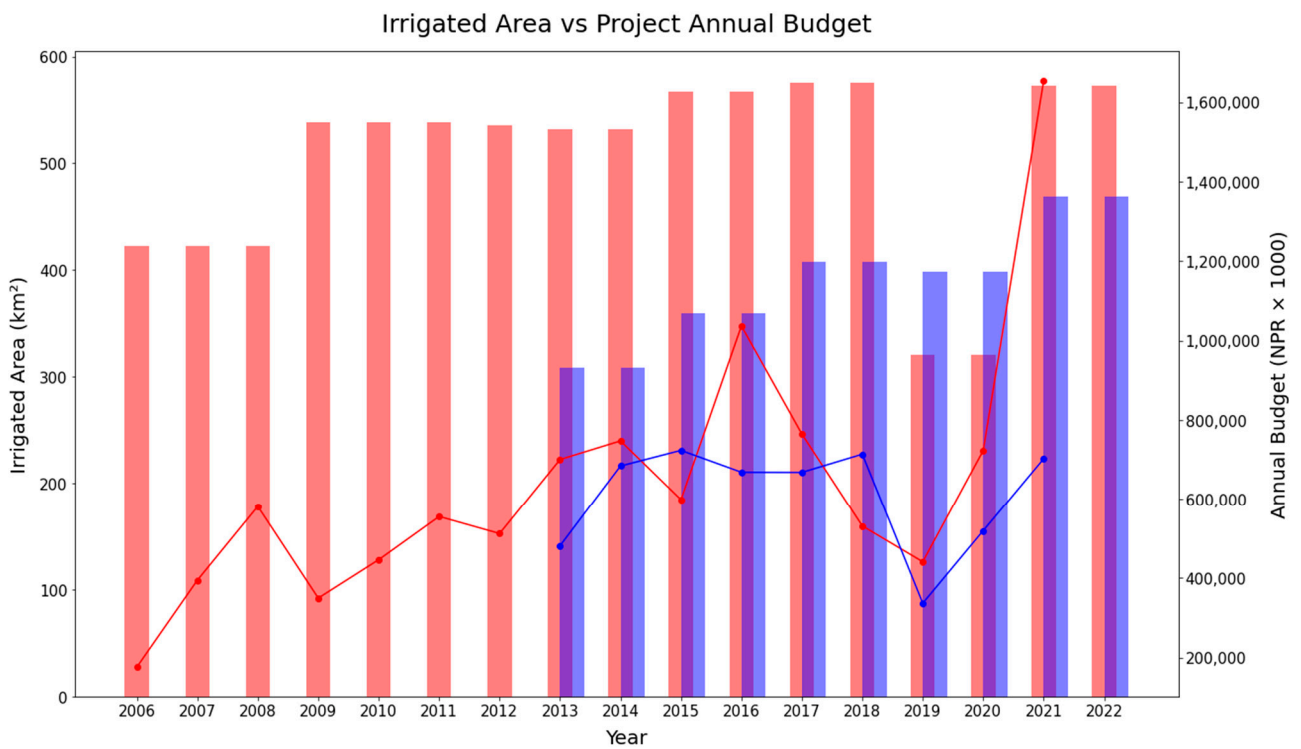


Figure 11. Impact of project's annual budget on Irrigated Area.

4.5.2. Variables Impacting Project Performance Project Annual Budget

The operation and maintenance of large irrigation projects like SMIP and BIS required a substantial amount of annual budgets, and variations in those funds had a significant impact on the performance of the projects. Figure 11 shows the time series of the annual budgets as well as the estimated irrigated areas in SMIP and BIS. An increasing trend in the allocation of annual budgets for SMIP can be observed from 2006–2007 to 2016–2017, while for BIS, a similar trend was seen only from 2013–2014 to 2014–2015 and then it was almost constant till 2018–2019. An increase in the irrigated area accompanied those periods of increased or constant budget allocation. Conversely, a decline in the budget can be observed for SMIP from 2016–2017 to 2019–2020 and for BIS, from 2018–2019 to 2019–2020, which corresponded to a decrease in the irrigated area.

Furthermore, after 2019–2020, an increase in the budget was followed by a corresponding increase in the irrigated area for both projects. In particular, in SMIP, the annual budget allocated for 2021–2022 is twice as much as the amount allocated in 2020–2021. This increased budget was primarily directed toward repairing the canals damaged by floods with a specific focus on constructing the damaged aqueduct.

Discharge of Main Canal

The fluctuations in the discharge diverted to the main canal had a minimal impact on the irrigated area of the project, as shown in Figure 12. Although the discharge in the main canal of SMIP was fluctuating, the irrigated area remained relatively constant throughout the study period, except for a decrease in the irrigated area for the years 2019–2020 and 2020–2021 due to the damage caused by flood, as explained in Section 4.2. Despite the variations in the main canal discharge, water management plans were implemented correctly and the project effectively managed the irrigation system.

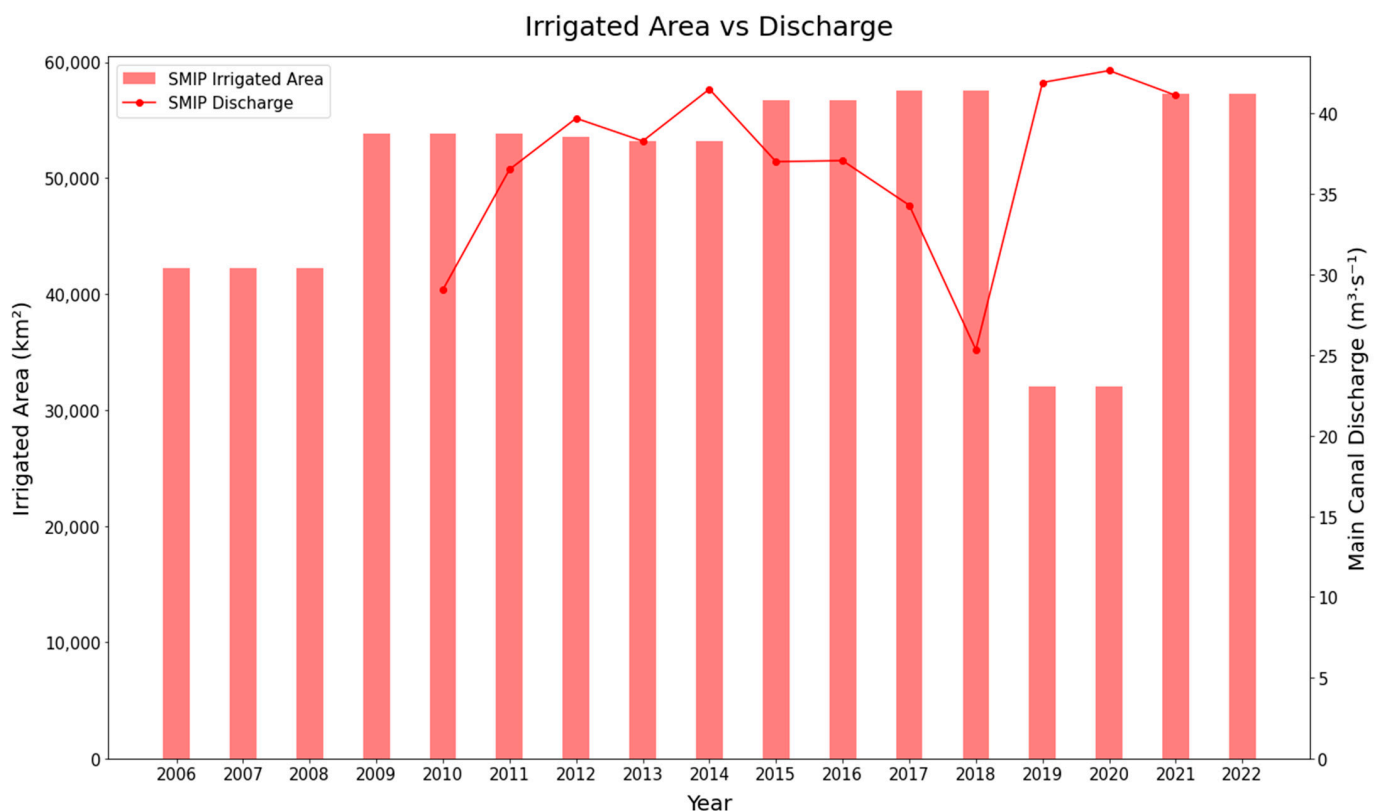


Figure 12. Impact of discharge of main canal on Irrigated Area.

Amount of Precipitation

The data of precipitation amounts were collected from the rainfall stations within the command area or the ones that had the runoff contribution to the command area of SMIP. Figure 13 shows how the variation in rainfall amount in the rainfall stations was related to the irrigated area. From 2006–2007 to 2010–2011, an increase in rainfall within the command area also led to an increase in the irrigated area. Despite a decreasing trend in rainfall from 2010–2011 to 2018–2019, the irrigated area remained almost constant, indicating effective water management and overall system management. However, a significant increase in rainfall occurred in 2019–2020 and 2020–2021, causing floods and damaging the irrigation system, which resulted in a substantial drop in the irrigated area.

Command Area Average Rainfall vs Irrigated Area

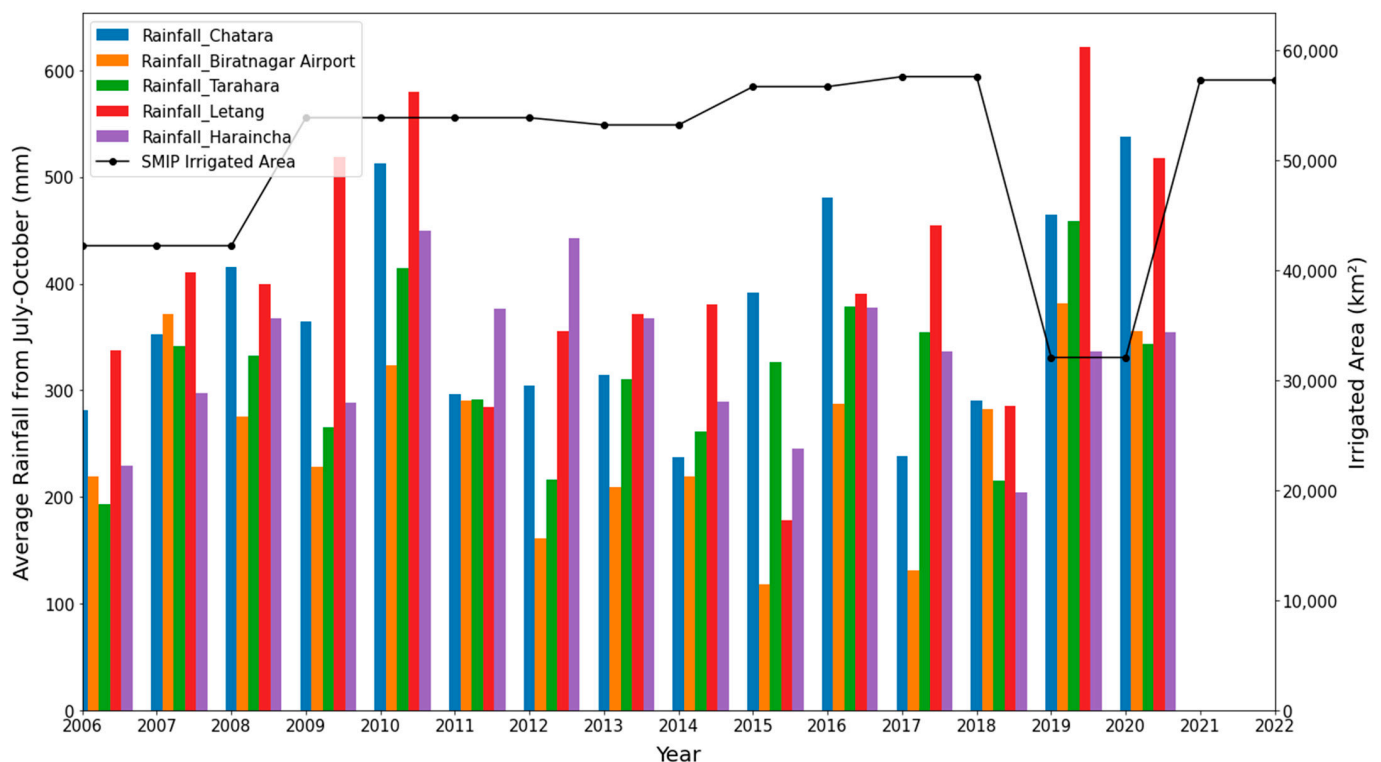


Figure 13. Variation in precipitation amount with Irrigated Area.

5. Discussion

Classifiers for cropland detection were trained and validated using training data collected from visual interpretation of Landsat and Google Earth images by [1,2,9]. In this study, we utilized training data from Landsat 8 OLI 2021–2022 and Google Earth images, validated using ground truth points, thus offering local relevance and accurate results. The producer's accuracy we obtained in this classification for the Agriculture class of 79% was comparable with [1] for the irrigated class, which was 80%. Our obtained accuracy is also comparable with the global study [2], which ranged from 70.3% to 86.4% for cropland.

The method we employed in this study provides a real-world representation of spatial patterns of irrigated areas, allows scalability, and reduces cost compared to the use of ground truth points alone, as conducted by [18]. However, the overall accuracy and kappa statistics of [18], which are 90.6% and 0.82, respectively, were higher than our method. Note that we trained our classifier using visual interpretation of images and validated it using ground truth data, so that our training and validation data come from different sources. This problem setting may make it more difficult to obtain better accuracies than [18], in which both training and validation data came from ground truth points.

In Sub-Saharan Africa, over-optimistic planning as a response to political pressure results in poor projections, over-promising benefits, and underestimating costs [1]. Similarly, in Nepal, the same reason has caused overestimation and under-delivering as far as the official record of the irrigated area is concerned in the case of SMIP. Regarding irrigation system management, SMIP demonstrates strong performance in its ability to recover swiftly from significant flooding events that caused a decline in the irrigated area during the 2019–2020 and 2020–2021 periods. BIS exhibits consistent improvement in performance, specifically regarding the expansion of the irrigated area, throughout the study period. These observations highlight the favorable performance of both SMIP and BIS compared to Sub-Saharan African irrigation projects shown in [1].

This study demonstrates that effective management has played a pivotal role in maintaining a consistent irrigated area for the irrigation projects. In the global context, there is growing concern over the impacts of global warming and climate change, which have led to an increase in the frequency, duration, and intensity of hydrological extremes, such as short-term extreme precipitation events, flash floods, and droughts worldwide [60–64]. It is worth noting that, in this study, we did not explore the direct effects of climate change on the performance of irrigation systems. However, it is a compelling area for future research to investigate how climate change could potentially impact irrigation projects in this region.

The globally trained cropland classification map [2] substantially overestimates cropland areas and is inconsistent with our locally trained cropland maps. Therefore, for accurate local or regional performance assessments of cropland classification, relying solely on globally trained results is not advisable.

In this study, the performance of the irrigation project was assessed using both socio-economic performance indicators (yield and ISF) and factors influencing the project's performance (project annual budget, main canal discharge, and precipitation levels). For a more comprehensive evaluation of the irrigation project, the inclusion of remote-sensing-based indicators, such as relative evapotranspiration, depleted fraction, delivery performance ratio, drainage ratio, and crop water productivity, as suggested by [19–22], alongside the existing indicators used in this study could be considered.

Only one growing season is considered in this study, as performed by [9,18,22,23]. Paddy, as used by [22,23], the staple food crop in developing countries, is used for the analysis in this study for one growing season. While we have focused on mapping the irrigated areas for paddy at a local level, a similar methodology of cropland mapping can be performed on regional and local scales for diverse crop types, extending beyond the scope of the current study.

The accuracy of the classifier employed in this study yielded favorable results; however, there may be some misclassifications in the classified maps. It is evident from Figure 3 that there is spectral similarity between the Agriculture class and the Forest/Pastures class, which may have caused misclassification of pixels under the Agriculture class as the Forest/Pastures class and vice versa. This could have led to poor accuracy due to the mixed-class problem. A potential solution to address this issue could be conducting a multi-temporal study of the irrigated area on different dates within a single growing season, as suggested by [10]. Additionally, other factors influencing classification accuracy, such as the number of classes, training sample size, size of the selected region of interest (ROI), satellite image quality, and the choice of classifier [65], should also be considered.

Most of the study period considered in this research, spanning from July to October, fell within the monsoon season, leading to significant cloud coverage issues. Since optical sensors, Landsat 5 TM and Landsat 8 OLI, were leveraged for this study, the imageries used were substantially affected by cloud cover, which, in turn, impacted the accuracy of cropland mapping. As Synthetic Aperture Radar (SAR) data can penetrate cloud cover, combining optical and radar data may offer a solution to obtain more accurate cropland classification maps in regions where cloud coverage poses a significant challenge [10,66–68].

It would be intriguing to conduct a comparison between the classification outcomes achieved in this study and those obtained through the implementation of alternative

methodologies, such as transfer learning, which considers the spatial diversity of class distributions [69], and deep learning approaches, which can effectively handle substantial training datasets [70]. Complex quantitative analysis of various climatic and economic factors (other than the ones discussed in this study) and socio-political factors governing scheme performance is promising for future works.

This study has provided accurate and up-to-date data on irrigated areas within the irrigation project, which is crucial for decision makers and stakeholders. The information regarding cropland changes over the years and the performance of the irrigation project can benefit both the Project Manager and the Water User's Association. It can assist in improving the monitoring of irrigated agricultural areas, coordinating managerial plans and policies related to croplands, enhancing agricultural water management, optimizing crop scheduling, and preparing crop calendars.

6. Conclusions

Despite significant implications for national policy, project annual budgets, and donor funding, the objective recording of irrigated areas in Nepal has been lacking. Therefore, this study addressed this gap by developing a locally trained machine-learning-based cropland map. Through the analysis of cropland dynamics, this research sheds light on the changes in the cropped area within Nepal's two largest irrigation projects, namely the Sunsari–Morang Irrigation Project (SMIP) and the Bagmati Irrigation System (BIS), spanning from 2006 to 2022. The results reveal that the DWRI overestimated the irrigated area for SMIP throughout the entire study period. In contrast, the satellite-derived irrigated area exceeded the data records for 2017–2018 and 2021–2022 in the case of BIS.

The accuracy assessment showed an overall accuracy of 82.2% and a kappa coefficient of 0.72, with producer's and consumer's accuracies for the Agriculture class, the class used to separate irrigated from the non-irrigated areas, were 79% and 96%, respectively. The thorough assessment of the performance of the irrigation project was performed in a cost-effective and timely manner. This method can be employed by the DWRI, Nepal, as an assessment method for other irrigation projects throughout the country.

This study also evaluated the importance of locally calibrated cropland maps. We discovered that only locally trained maps, compared to global cropland classification maps, could accurately replicate the precise allocation of irrigated land at a small scale. Therefore, these maps are necessary for conducting performance assessments of irrigation projects at the local level.

As a follow-up to this study, our intention is to employ similar methodologies to generate an updated, regionally trained, high-resolution seasonal cropland classification map of Nepal, leveraging the capabilities of Sentinel-2 imagery. This effort is motivated by the current lack of detailed, high-resolution cropland maps for the region, with only a coarser resolution map utilizing MODIS NDVI time series [25] currently available.

Author Contributions: Conceptualization, A.N. and Y.S.; methodology, A.N.; software, A.N.; formal analysis, A.N. and Y.S.; investigation, A.N.; resources, Y.S.; data curation, A.N.; writing—original draft preparation, A.N.; writing—review and editing, A.N. and Y.S.; visualization, A.N.; supervision, Y.S.; project administration, A.N.; funding acquisition, Y.S. All authors have read and agreed to the published version of the manuscript.

Funding: This study was supported by the KAKENHI grant 21H01430 and JAXA grant ER3AMF106.

Acknowledgments: We acknowledge the SMIP project team for providing project-specific data, and DHM, Nepal, for providing the precipitation data.

Conflicts of Interest: The authors declare no conflict of interest.

References

1. Higginbottom, T.P.; Adhikari, R.; Dimova, R.; Redicker, S.; Foster, T. Performance of Large-Scale Irrigation Projects in Sub-Saharan Africa. *Nat. Sustain.* **2021**, *4*, 501–508. [[CrossRef](#)]

2. Potapov, P.; Turubanova, S.; Hansen, M.C.; Tyukavina, A.; Zalles, V.; Khan, A.; Song, X.-P.; Pickens, A.; Shen, Q.; Cortez, J. Global Maps of Cropland Extent and Change Show Accelerated Cropland Expansion in the Twenty-First Century. *Nat. Food* **2022**, *3*, 19–28. [[CrossRef](#)] [[PubMed](#)]
3. Tariq, A.; Yan, J.; Gagnon, A.S.; Riaz Khan, M.; Mumtaz, F. Mapping of Cropland, Cropping Patterns and Crop Types by Combining Optical Remote Sensing Images with Decision Tree Classifier and Random Forest. *Geo-Spat. Inf. Sci.* **2022**, 1–19. [[CrossRef](#)]
4. Cosgrove, W.J.; Loucks, D.P. Water Management: Current and Future Challenges and Research Directions. *Water Resour. Res.* **2015**, *51*, 4823–4839. [[CrossRef](#)]
5. Vörösmarty, C. Global Water Assessment and Potential Contributions from Earth Systems Science. *Aquat. Sci.* **2002**, *64*, 328–351. [[CrossRef](#)]
6. Alcamo, J.; Döll, P.; Henrichs, T.; Kaspar, F.; Lehner, B.; Rösch, T.; Siebert, S. Global Estimates of Water Withdrawals and Availability under Current and Future “Business-as-Usual” Conditions. *Hydrol. Sci. J.* **2003**, *48*, 339–348. [[CrossRef](#)]
7. Boucher, O.; Myhre, G.; Myhre, A. Direct Human Influence of Irrigation on Atmospheric Water Vapour and Climate. *Clim. Dyn.* **2004**, *22*, 597–603. [[CrossRef](#)]
8. Bendini, H.; Sanches, I.; Körting, T.; Fonseca, L.; Luiz, A.; Formaggio, A. Using landsat 8 image time series for crop mapping in a region of Cerrado, Brazil. *ISPRS Int. Arch. Photogramm. Remote Sens. Spat. Inf. Sci.* **2016**, *41*, 845–850. [[CrossRef](#)]
9. Traoré, F.; Bonkougou, J.; Compaoré, J.; Kouadio, L.; Wellens, J.; Hallot, E.; Tychon, B. Using Multi-Temporal Landsat Images and Support Vector Machine to Assess the Changes in Agricultural Irrigated Areas in the Mogtiedo Region, Burkina Faso. *Remote Sens.* **2019**, *11*, 1442. [[CrossRef](#)]
10. Koley, S.; Chockalingam, J. Sentinel 1 and Sentinel 2 for Cropland Mapping with Special Emphasis on the Usability of Textural and Vegetation Indices. *Adv. Space Res.* **2022**, *69*, 1768–1785. [[CrossRef](#)]
11. Pittman, K.; Hansen, M.C.; Becker-Reshef, I.; Potapov, P.V.; Justice, C.O. Estimating Global Cropland Extent with Multi-Year MODIS Data. *Remote Sens.* **2010**, *2*, 1844–1863. [[CrossRef](#)]
12. Traoré, F.; Cornet, Y.; Denis, A.; Wellens, J.; Tychon, B. Monitoring the Evolution of Irrigated Areas with Landsat Images Using Backward and Forward Change Detection Analysis in the Kou Watershed, Burkina Faso. *Geocarto Int.* **2013**, *28*, 733–752. [[CrossRef](#)]
13. Gumma, M.K.; Thenkabail, P.S.; Hideto, F.; Nelson, A.; Dheeravath, V.; Busia, D.; Rala, A. Mapping Irrigated Areas of Ghana Using Fusion of 30 m and 250 m Resolution Remote-Sensing Data. *Remote Sens.* **2011**, *3*, 816–835. [[CrossRef](#)]
14. Knauer, K.; Gessner, U.; Fensholt, R.; Forkuor, G.; Kuenzer, C. Monitoring Agricultural Expansion in Burkina Faso over 14 Years with 30 m Resolution Time Series: The Role of Population Growth and Implications for the Environment. *Remote Sens.* **2017**, *9*, 132. [[CrossRef](#)]
15. Ambika, A.K.; Wardlow, B.; Mishra, V. Remotely Sensed High Resolution Irrigated Area Mapping in India for 2000 to 2015. *Sci. Data* **2016**, *3*, 160118. [[CrossRef](#)] [[PubMed](#)]
16. Shahriar Pervez, M.; Budde, M.; Rowland, J. Mapping Irrigated Areas in Afghanistan over the Past Decade Using MODIS NDVI. *Remote Sens. Environ.* **2014**, *149*, 155–165. [[CrossRef](#)]
17. Gumma, M.K.; Thenkabail, P.S.; Nelson, A. Mapping Irrigated Areas Using MODIS 250 Meter Time-Series Data: A Study on Krishna River Basin (India). *Water* **2011**, *3*, 113–131. [[CrossRef](#)]
18. Falanga Bolognesi, S.; Pasolli, E.; Belfiore, O.R.; De Michele, C.; D’Urso, G. Harmonized Landsat 8 and Sentinel-2 Time Series Data to Detect Irrigated Areas: An Application in Southern Italy. *Remote Sens.* **2020**, *12*, 1275. [[CrossRef](#)]
19. Awan, U.K.; Tischbein, B.; Conrad, C.; Martius, C.; Hafeez, M. Remote Sensing and Hydrological Measurements for Irrigation Performance Assessments in a Water User Association in the Lower Amu Darya River Basin. *Water Resour. Manag.* **2011**, *25*, 2467–2485. [[CrossRef](#)]
20. Sawadogo, A.; Kouadio, L.; Traoré, F.; Zwart, S.J.; Hessels, T.; Gündoğdu, K.S. Spatiotemporal Assessment of Irrigation Performance of the Kou Valley Irrigation Scheme in Burkina Faso Using Satellite Remote Sensing-Derived Indicators. *ISPRS Int. J. Geo-Inf.* **2020**, *9*, 484. [[CrossRef](#)]
21. Zwart, S.J.; Leclert, L.M.C. A Remote Sensing-Based Irrigation Performance Assessment: A Case Study of the Office Du Niger in Mali. *Irrig. Sci.* **2010**, *28*, 371–385. [[CrossRef](#)]
22. Bandara, K.M.P.S. *Assessing Irrigation Performance by Using Remote Sensing*; ITC dissertation; ITC: Enschede, The Netherlands, 2006; ISBN 978-90-8504-406-2.
23. Kumar, K.A. Irrigation Performance Assessment of Left Bank Canal, Nagarjuna Sagar Project, India During Rabi Using Remote Sensing and GIS. *Agrotechnology* **2014**, *3*, 2. [[CrossRef](#)]
24. Nikam, B.R.; Garg, V.; Thakur, P.K.; Aggarwal, S.P. Application of Remote Sensing and GIS in Performance Evaluation of Irrigation Project at Disaggregated Level. *J. Indian Soc. Remote Sens.* **2020**, *48*, 979–997. [[CrossRef](#)]
25. Rimal, B.; Zhang, L.; Rijal, S. Crop Cycles and Crop Land Classification in Nepal Using MODIS NDVI. *Remote Sens. Earth Syst. Sci.* **2018**, *1*, 14–28. [[CrossRef](#)]
26. Gumma, M.K.; Gauchan, D.; Nelson, A.; Pandey, S.; Rala, A. Temporal Changes in Rice-Growing Area and Their Impact on Livelihood over a Decade: A Case Study of Nepal. *Agric. Ecosyst. Environ.* **2011**, *142*, 382–392. [[CrossRef](#)]
27. Paudel, B.; Zhang, Y.; Li, S.; Liu, L. Spatiotemporal Changes in Agricultural Land Cover in Nepal over the Last 100 Years. *J. Geogr. Sci.* **2018**, *28*, 1519–1537. [[CrossRef](#)]

28. Mishra, A.K.; Aithal, P.S. Performance Assessment of Irrigation: A Case from Nepal-Asia. *Int. J. Manag. Technol. Soc. Sci.* **2022**, *7*, 444–464. [CrossRef]
29. Lam, W.F. Improving the Performance of Small-Scale Irrigation Systems: The Effects of Technological Investments and Governance Structure on Irrigation Performance in Nepal. *World Dev.* **1996**, *24*, 1301–1315. [CrossRef]
30. Sapkota, A.; Pandit, H.P.; Shrestha, R. Hydraulic and Sediment Handling Performance Assessment of Rani Jamara Kulariya Irrigation Project (RJKIP) by Conjunctive Use of 1D and 3D Simulation Models. *Naresuan Univ. Eng. J.* **2016**, *11*, 1–6.
31. IrrigationYearBook2010.11. Available online: <https://www.dwri.gov.np/files/notice/20210804064529.pdf> (accessed on 20 June 2023).
32. IrrigationYearBook2011.12. Available online: <https://www.dwri.gov.np/files/notice/20210804065111.pdf> (accessed on 20 June 2023).
33. IrrigationYearBook2012.13. Available online: <https://www.dwri.gov.np/files/notice/20210804065143.pdf> (accessed on 20 June 2023).
34. IrrigationYearBook2013.14. Available online: <https://www.dwri.gov.np/files/notice/20210804065226.pdf> (accessed on 20 June 2023).
35. IrrigationYearBook2014.15. Available online: <https://www.dwri.gov.np/files/notice/20210804065257.pdf> (accessed on 20 June 2023).
36. IrrigationYearBook2015.16. Available online: <https://www.dwri.gov.np/files/notice/20210804065358.pdf> (accessed on 20 June 2023).
37. IrrigationYearBook2016.17. Available online: <https://www.dwri.gov.np/files/notice/20210804065428.pdf> (accessed on 20 June 2023).
38. IrrigationYearBook2017.18. Available online: <https://www.dwri.gov.np/files/notice/20210804070853.pdf> (accessed on 20 June 2023).
39. IrrigationYearBook2018.19. Available online: <https://www.dwri.gov.np/files/notice/20210804090308.pdf> (accessed on 20 June 2023).
40. IrrigationYearBook2019.20. Available online: <https://www.dwri.gov.np/files/notice/20210804090444.pdf> (accessed on 20 June 2023).
41. IrrigationYearBook2021.22. Available online: <https://pdf.ac/39UuAy> (accessed on 20 June 2023).
42. Landsat 5 | U.S. Geological Survey. Available online: <https://www.usgs.gov/landsat-missions/landsat-5> (accessed on 15 July 2023).
43. Landsat 8 | U.S. Geological Survey. Available online: <https://www.usgs.gov/landsat-missions/landsat-8> (accessed on 15 July 2023).
44. Shelestov, A.; Lavreniuk, M.; Kussul, N.; Novikov, A.; Skakun, S. Exploring Google Earth Engine Platform for Big Data Processing: Classification of Multi-Temporal Satellite Imagery for Crop Mapping. *Front. Earth Sci.* **2017**, *5*. [CrossRef]
45. Gorelick, N.; Hancher, M.; Dixon, M.; Ilyushchenko, S.; Thau, D.; Moore, R. Google Earth Engine: Planetary-Scale Geospatial Analysis for Everyone. *Remote Sens. Environ.* **2017**, *202*, 18–27. [CrossRef]
46. Jensen, J.R. *Introductory Digital Image Processing: A Remote Sensing Perspective*; Pearson Education: Upper Saddle River, NJ, USA, 2015; ISBN 978-0-13-439516-6.
47. Thenkabail, P.; Teluguntla, P.; Biggs, T.; Gumma, M.; Turrall, H. Spectral Matching Techniques to Determine Historical Land Use/Land Cover (LULC) and Irrigated Areas Using Time-Series AVHRR Pathfinder Datasets in the Krishna River Basin, India. *Photogramm. Eng. Remote Sens.* **2007**, *73*, 1029–1040.
48. Liu, X.; Skidmore, A.; Oosten, H. Integration of Classification Methods for Improvement of Land-Cover Map Accuracy. *ISPRS J. Photogramm. Remote Sens.* **2002**, *56*, 257–268. [CrossRef]
49. Liu, C.; Frazier, P.; Kumar, L. Comparative Assessment of the Measures of Thematic Classification Accuracy. *Remote Sens. Environ.* **2007**, *107*, 606–616. [CrossRef]
50. Smits, P.C.; Dellepiane, S.G.; Schowengerdt, R.A. Quality Assessment of Image Classification Algorithms for Land-Cover Mapping: A Review and a Proposal for a Cost-Based Approach. *Int. J. Remote Sens.* **1999**, *20*, 1461–1486. [CrossRef]
51. Lunetta, R.S. Remote Sensing and Geographic Information System Data Integration: Error Sources and Research Issues. *Photogramm. Eng.* **1991**, *57*, 677–687.
52. Islami, F.A.; Tarigan, S.D.; Wahjunie, E.D.; Dasanto, B.D. Accuracy Assessment of Land Use Change Analysis Using Google Earth in Sadar Watershed Mojokerto Regency. *IOP Conf. Ser. Earth Environ. Sci.* **2022**, *950*, 012091. [CrossRef]
53. Congalton, R.G. A Review of Assessing the Accuracy of Classifications of Remotely Sensed Data. *Remote Sens. Environ.* **1991**, *37*, 35–46. [CrossRef]
54. STATISTICAL-INFORMATION-ON-NEPALESE-AGRICULTURE-2071-72. Available online: <https://moald.gov.np/wp-content/uploads/2022/04/STATISTICAL-INFORMATION-ON-NEPALESE-AGRICULTURE-2071-72.pdf> (accessed on 16 July 2023).
55. STATISTICAL-INFORMATION-ON-NEPALESE-AGRICULTURE-2077-78. Available online: <https://moald.gov.np/wp-content/uploads/2022/07/STATISTICAL-INFORMATION-ON-NEPALESE-AGRICULTURE-2077-78.pdf> (accessed on 16 July 2023).
56. Agricultural-Statistics-Pocket-Book-2023-1.Pdf. Available online: <https://moald.gov.np/wp-content/uploads/2023/08/Agricultural-Statistics-Pocket-book-2023-1.pdf> (accessed on 12 September 2023).
57. NEPAL STATISTICAL YEAR BOOK. 2015. Available online: <https://nepalindata.com/resource/STATISTICAL-YEAR-BOOK-NEPAL-2015/> (accessed on 16 July 2023).
58. NEPAL STATISTICAL YEAR BOOK. 2021. Available online: <https://nepalindata.com/resource/NEPAL-STATISTICAL-YEAR-BOOK-2021/> (accessed on 16 July 2023).
59. The Himalayan Damage to Morang-Sunsari Irrigation Project Estimated at Rs 800mln. Available online: <https://thehimalayantimes.com/nepal/damage-morang-sunsari-irrigation-project-estimated-rs-800mln> (accessed on 15 July 2023).
60. Tabari, H.; Hosseinzadehtalaei, P.; Thiery, W.; Willems, P. Amplified Drought and Flood Risk Under Future Socioeconomic and Climatic Change. *Earths Future* **2021**, *9*, e2021EF002295. [CrossRef]
61. Prein, A.F.; Rasmussen, R.M.; Ikeda, K.; Liu, C.; Clark, M.P.; Holland, G.J. The Future Intensification of Hourly Precipitation Extremes. *Nat. Clim. Change* **2017**, *7*, 48–52. [CrossRef]
62. Zhang, Y.; Wang, Y.; Chen, Y.; Xu, Y.; Zhang, G.; Lin, Q.; Luo, R. Projection of Changes in Flash Flood Occurrence under Climate Change at Tourist Attractions. *J. Hydrol.* **2021**, *595*, 126039. [CrossRef]

63. Pachauri, R.K.; Allen, M.R.; Barros, V.R.; Broome, J.; Cramer, W.; Christ, R.; Church, J.A.; Clarke, L.; Dahe, Q.; Dasgupta, P.; et al. *Climate Change 2014: Synthesis Report. Contribution of Working Groups I, II and III to the Fifth Assessment Report of the Intergovernmental Panel on Climate Change*; Pachauri, R.K., Meyer, L., Eds.; IPCC: Geneva, Switzerland, 2014; p. 151. ISBN 978-92-9169-143-2.
64. Dai, A.; Zhao, T.; Chen, J. Climate Change and Drought: A Precipitation and Evaporation Perspective. *Curr. Clim. Change Rep.* **2018**, *4*, 301–312. [[CrossRef](#)]
65. Nguyen, H.T.T.; Doan, T.M.; Tomppo, E.; McRoberts, R.E. Land Use/Land Cover Mapping Using Multitemporal Sentinel-2 Imagery and Four Classification Methods—A Case Study from Dak Nong, Vietnam. *Remote Sens.* **2020**, *12*, 1367. [[CrossRef](#)]
66. Sonobe, R.; Yamaya, Y.; Tani, H.; Wang, X.; Kobayashi, N.; Mochizuki, K. Assessing the Suitability of Data from Sentinel-1A and 2A for Crop Classification. *GIScience Remote Sens.* **2017**, *54*, 918–938. [[CrossRef](#)]
67. Yang, H.; Pan, B.; Wu, W.; Tai, J. Field-Based Rice Classification in Wuhua County through Integration of Multi-Temporal Sentinel-1A and Landsat-8 OLI Data. *Int. J. Appl. Earth Obs. Geoinf.* **2018**, *69*, 226–236. [[CrossRef](#)]
68. Whyte, A.; Ferentinos, K.P.; Petropoulos, G.P. A New Synergistic Approach for Monitoring Wetlands Using Sentinels -1 and 2 Data with Object-Based Machine Learning Algorithms. *Environ. Model. Softw.* **2018**, *104*, 40–54. [[CrossRef](#)]
69. Pan, S.J.; Yang, Q. A Survey on Transfer Learning. *IEEE Trans. Knowl. Data Eng.* **2010**, *22*, 1345–1359. [[CrossRef](#)]
70. Zhu, X.X.; Tuia, D.; Mou, L.; Xia, G.-S.; Zhang, L.; Xu, F.; Fraundorfer, F. Deep Learning in Remote Sensing: A Comprehensive Review and List of Resources. *IEEE Geosci. Remote Sens. Mag.* **2017**, *5*, 8–36. [[CrossRef](#)]

Disclaimer/Publisher’s Note: The statements, opinions and data contained in all publications are solely those of the individual author(s) and contributor(s) and not of MDPI and/or the editor(s). MDPI and/or the editor(s) disclaim responsibility for any injury to people or property resulting from any ideas, methods, instructions or products referred to in the content.